Peer-reviewed version available at Materials 2019, 12, 1555; doi:10.3390/ma12091555

Article

Design of a 2 × 4 Hybrid MMI-MZI Configuration with MMI Phase-shifters

Boris B. Niraula[1,‡,*], and Conrad Rizal [2,†,‡]

1 SeedNanoTech and Consulting, Brampton, ON, Canada, L6Y 3J6 (boris.niraula@seednanotech.com)
2 Department of Electrical & Computer Engineering, The University of British Columbia, Vancouver, BC, Canada V6T 1Z4 (crizal@ece.ubc.ca)
* Correspondence: boris.b.niraula@gmail.com; Tel.: +1-289-499-3249
† Current address: Nanophotonics Laboratory, GEM Systems Inc., Markham, ON, Canada
‡ These authors contributed equally to this work.

Version April 22, 2019 submitted to Preprints

Abstract: This paper reports design of a 2 × 4 hybrid multimode interferometer-Mach-zehnder interferometer (MMI-MZI) configuration and compact thermo-optical switch consisting of slab waveguides on the silicon-on-insulator (SOI), platform. The device consisted of two identical MMIs as power splitters and couplers that are connected with two identical MMI-based phase shifters, and linear tapers at both ends of the MMIs to minimize the power coupling loss. A thin Al pad is used as a heating element, and a trench is created around this pad to prevent heat from spreading and to minimize loss. The calculated average thermo-optical switching power consumption, excess loss, and power imbalance are 1.4 mW, 0.9 dB, and 0.1 dB, respectively. The overall footprint of the device is 6 × 304 μm^2. The new heating method has advantages of compact size, ease of fabrication on SOI platform with the current CMOS technology, and offers low excess loss and power consumption as demanded by devices based on SOI technology. The device can act as two independent optical switches in one structure.

Keywords: Multimode interferometer, MMI, thermo-optical switch, SOI technology, biosensor.

1. Introduction

The consistent and continuous demand/growth of high-speed internet with a higher volume of data processing prompts the need for high-speed non-blocking optical switches with less sensitivity to polarization and operational wavelength [1]. These functionalities need to accompany with low power consumption, low loss, small device footprint, and a higher number of ports, full operational bandwidth that depends on the number of output ports, and low production cost.

The silicon-on-insulator (SOI) material platform supports the design of compact wave-guiding devices with reasonable fabrication tolerance and cost, and has attracted renewed research interest. The demand for high-speed internet and the vast amount of data transmission calls for a new generation of photonic switches. Interested readers in the comparison of technical characteristics of presently operational and proposed optical switches based on MMI waveguides are referred to [2].

Two widely known photonic waveguiding configurations are commonly used in realizing switching, modulating and filtering functionalities. These include Mach-zehnder interferometry (MZI) [3] and multimodal coupler-based interferometry (MMI) [4]. MZI-based waveguiding configurations consists of directional couplers (DCs), tappers and nano-sized optical wires of different dimensions and geometry [5] and operate over wide/broad optical bandwidth, and show environmental stability.

Most of the work reported in literature on optical switches have employed directional couplers (DC) as the power splitter and combiners where high-speed operation is achieved by varying the coupling co-efficient of the couplers. For high speed operation, the distance between the adjacent waveguides in the DC need to be small. However, that creates higher mode conversion optical losses,

which is undesirable. The overall footprint of the DC is also large. In addition, most nano-sized waveguides used in DC have small fabrication tolerance and therefore, a tight control of the fabrication process is necessary.

MMIs offer benefits over DCs due to their advantages of compactness, ease of fabrication, wide band operation, large fabrication tolerance (up to $\pm$ 50 nm can be achieved). Further, the silicon photonic platform enables the possibility of fabricating and integrating the optical device with the electronics on the same platform in the commentary metal-oxide-semiconductor (CMOS) environment. This enables large-scale integration of photonic devices at a lower cost and higher volume production using CMOS-compatible fabrication method. In this regard, a MMI power coupler/splitter plays an important role in the development of integrated photonics due to above-mentioned merits.

MMI-based wave-guiding configurations consist of micro-sized slab-like couplers/decouplers with connectors of different shape and geometry [4]. The MMI couplers work on the principle of self-imaging effect [6]. In addition, MMI-based couplers/decouplers as switching configurations offer advantages such as well-defined decoupling/coupling ratios, lower excess loss, low polarization sensitivity, better dimensional tolerance and/or ease of fabrication, and ease of cascading them and integration with the CMOS technology, wavelength insensitive transmission spectra, and support many ports. However, the coupling ratios of the MMI splitters/couplers are very limited to the fixed coupling ratios if only one of the MMIs is used for operation. The fixed coupling/splitting ratios would allow only a limited applications in all-optical signal processing and optical networks. Therefore, it is highly desired to implement the couplers with variable coupling ratios. This can be achieved using phase shifters, in this case, two MMI phase shifters are added to the MZI arms to control the phase of the propagating waves.

In this paper, we have theoretically demonstrated all MMI based 2 $\times$ 4 configurations in which two separate MMI decouplers/couplers (each with 6 μm $\times$ 140 μm) are connected via two MMI-based phase shifters (each with 2 μm $\times$ 8 μm) within a compact footprint using 4 μm long tapered waveguides. The most important feature of this device is that it can act as two independent optical switches in a single device where the coupling ratios of the device can be readily varied by using two independent phase shifters. The working principle of the device is verified using the transfer matrix method and FDTD simulation tools. As demonstrated earlier in Ref [7], an Al heating element is incorporated in the phase shifter arms to realize thermo-optical switching.

2. Design, Simulation, and Optimization

2.1. Multimode Interferometers

The fundamental switching element in this work is MMI based phase shifters and thermo-optic based heaters. As shown in Fig. 1, the design of the MMIs is based on SOI technology. The device consisted of two identical MMIs: MMI_1 and MMI_2, each with 140 μm $\times$ 6 μm dimension, connected via two smaller phase shifters MMI_3 and MMI_4, each with 16 μm^2 and a metal heating element incorporated in them (Information on thermo-optic effect will be discussed in Section 2.4). The MMI_1, in this case, is designed to act as a power decoupler whereas MMI_2 is designed as a power coupler.

The design of the 2 $\times$ 4 optical switch considered in this paper is based on single MMI couplers/splitters and their cascaded operation, the operation principle of which is based on self-imaging theory and total internal reflection [6,8–17]. Further information on principle of operation is given in 3. Fig. 1 presents an illustrative configuration of the device that contains one 3-dB input MM1, two phase shifters, one at each arm of the MMI, and a 3-dB MMI couplers/splitters. The MMIs are designed in such a way that when the input signal is fed through a_{i1}, the output power is equally split between a_{o1}, and a_{o4}. Likewise, then the input signal is fed through the port a_{i2}, the output power is equally split between a_{o2}, and a_{o3}. So each MMIs can act as two independent devices.

Based on self-imaging properties, a prototype MMI 3-dB power splitter/combiner is first designed. According to [6], the beat length, L_π between lowest order modes of an MMI is given by:

$$L_\pi = \frac{\pi}{(\beta_o - \beta_1)}), \tag{1}$$

where, β_0 and β_1 denote the propagation constants of the fundamental and first mode, respectively. As explained by Ulrich [17] and Soldano [13], self-imaging is achieved when the input field is reproduced as single or multiple images along the dimension of the MMI slab at a periodic interval. Since the light beam is confined in an MMI slab because of obeying total multiple reflections, the beam undergoes multiple periodically repeating self-interference patterns. For instance, self-generation of two interference patterns with equal output powers can be achieved using the relationship as [6]:

$$L_{MMI} = M \times 3 \times \frac{L_\pi}{N}, \tag{2}$$

where M and N are any positive integers without a common divisor, N is the number of self-replicating interferences, and M defines device length with various N [16]. The relationship in (2) suggests that a compact device is obtained for M = 1. For the MMI with the effective width, W_e and effective refractive index, N_{eff}, and when excited from either input or output ports, the L_π can also be given by:

$$L_\pi = \frac{{W_e}^2 \times 4 \times N_{eff}}{(3 \times \lambda)}. \tag{3}$$

That means, L_π is related to the effective width, λ, and N_{eff}. For a lateral wave guided structure, the W_e is related to the geometric width of the device as [13]:

$$W_e = W_{MMI} + \frac{\lambda}{\pi}\left(\frac{N_{core}}{N_{cld}}\right)^2 \frac{1}{\sqrt{({N_{core}}^2 + {N_{cld}}^2)}}, \tag{4}$$

where N_{core} and N_{cld} are the refractive index of core and cladding layers, respectively. At one beat length and a half, the MMI produces a pair of identical images, making the waveguide a 3_{dB} coupler.

As shown in Fig. 1, the device is designed to act as two independent optical switches with four output and two input tapered ports (the tapered section is shown in the inset at the middle top for clarity and the cross-sectional view of the wave guide is shown at the top right). Air, with a refractive index of 1.0 is considered as the upper cladding whereas SiO_2, with a refractive index of 1.45 as the lower cladding. The individual MMI device characteristics were estimated using MATLAB mode solver [18] and FDTD simulation tool with TE polarized (s-polarized) light at λ = 1550 nm. The calculated geometrical parameters of the MMI couplers/decouplers are given in Table 1.

Table 1. Geometrical and optical characteristics of the MMI Decouplers/Couplers, access waveguides (AWs), and MMI phase shifters (PS) obtained from simulation. The symbols W, L, and t denote width, length, and thickness/height of the device, respectively. Optical parameters used for simulation include substrate, Si (n=3.48), lower cladding, SiO_2 (n=1.45), core, Si (n=3.48), and upper cladding, air (n = 1.0).

Components	Width (μm)	Length (μm)	Height (μm)
MMIs: MMI_1, MMI_2	W_{MMI} = 6.0	L_{MMI} = 140	t_{MMI} = 0.22
Access Waveguides, AWs	W_{AW} = 0.5 - 8.0	L_{AW} = 4	t_{AW} = 0.22
PSs: MMI_3, MMI_4	W_{PS} = 2	L_{PS} = 8	t_{PS} = 0.22

Peer-reviewed version available at Materials 2019, 12, 1555; doi:10.3390/ma12091555

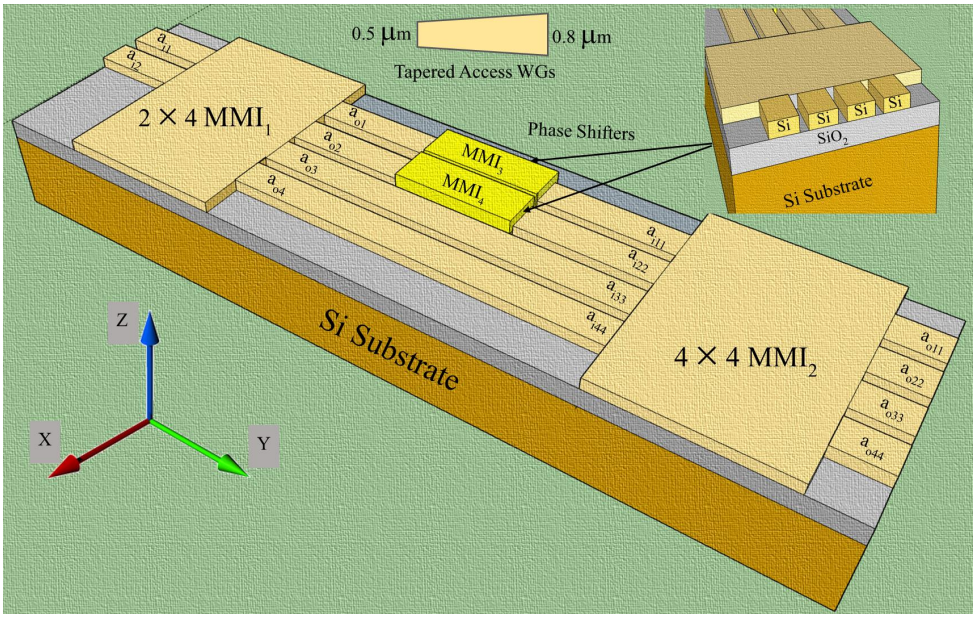

Figure 1. Schematics of the MMI device: Decoupler (MMI_1) and Coupler (MMI_2). The inset in the top middle shows a tapered access waveguide and in the top right the cross-sectional view of the MMIs. Input ports: a_{i1} and a_{i2} of MMI_1 and output ports: a_{o11}, a_{o22}, a_{o33}, and a_{o44} of MMI_2.

2.2. Access Waveguides

To ensure single mode operation, geometrical parameters of the access waveguides were derived using MATLAB mode solver [18] for the TE polarized (s-polarized) light at λ = 1550 nm and FDTD simulation tool. The core thickness of 0.22 μm and access waveguide width of 0.5 μm at the input side of the tapered waveguide were chosen to achieve single mode operation. All the calculated geometrical parameters of the access waveguides are given in Table 1.

2.3. Phase Shifters

In many circumstances, the phase shifting is an essential characteristic of the optical signal as it traverses through waveguides, including switches and filters. Not all kind of phase shifting is, however, useful for switching application. In most cases, the desired phase shift requires special device design consideration. In the present work, two 1 × 1 MMI devices (MMI_3 and MMI_4) are considered for phase shifting purpose.

The calculated widths of the MMI_3 and MMI_4, designed as a 1 × 1 phase shifters, corresponding to the MMI lengths chosen to form a single image at the output. In the simulation, the length of the MMIs were varied from 0 to 10 μm to obtain corresponding MMI width for single mode operation. The width was kept to 2 μm for a 8 μm long MMI to avoid cross-talk between the adjacent waveguides. The chosen waveguide can support up to a maximum of 3 optical modes. These parameters were obtained from the FDTD simulation as well as MATLAB Mode solver [18]. The grid-size used during FDTD simulation was 5 nm. In analogy to reference [7], two mesh override regions were used. The calculated parameters of the phase shifter are given in Table 1.

2.4. Thermo-optic Heaters

The change in refractive index along the length of an optical waveguide leads to change in mode propagation constant of the optical signal. Refractive index of a Si waveguide can be tuned using two effects: free career plasma dispersion and thermo-optical effect [7]. The thermo-optical effect is relatively stronger as Si exhibits a strong thermo-optical coefficient of $\frac{dn}{dT}$ = -1.8 × 10^{-04} /K at 300 K.

Table 2. Physical properties of the waveguide and heater element.

SN	Material	Therm. Conductivity, W/(m.K)	Heating coefficient (/K)
1	Si	163.25	160×10^{-06}
2	SiO_2	1.405	8×10^{-06}
3	Al	204	24×10^{-06}

3. Principle of Operation of the Device

The operating principle of the thermo-optic switch is based on the change of mode propagation constant of the beam as it propagates through the phase-shifter/modulating arm with respect to the reference arm. The optical transfer function of this switch is governed by the multimode interference principle that is achieved by modulating the phases of the transmitted light. The device's input signal can be switched to either output of the device when the phase difference, changes from 0 to π between the MMI arms. A thin Al pad is introduced in both the phase shifter arms, MMI_3 and MMI_4, with the aim of tuning/varying the coupling coefficient at the output ports. Either one or both phase shifters can be tuned depending on the application to realize the desired phase shift. Since the design and realization of the thermo-optical switch requires several practical considerations, the optical field and mode propagation profiles of the individual MMIs are studied as a first step. This is further discussed in the Section 4.

The phase difference ($\Delta\phi$) between the light propagating through the phase modulating and reference arms depends strongly on the the dimension of the waveguide and is given as [7]:

$$\Delta\phi = \frac{2\pi}{\lambda} \times (\Delta n_{eff} \times L_{MMI}) \tag{5}$$

where λ is the operating wavelength, 1550 nm in this case, Δn_{eff} is the change in refractive indices, and L_{MMI} is the length of the modulating arm. Various parameters of the waveguides and heater element are given in Table 2.

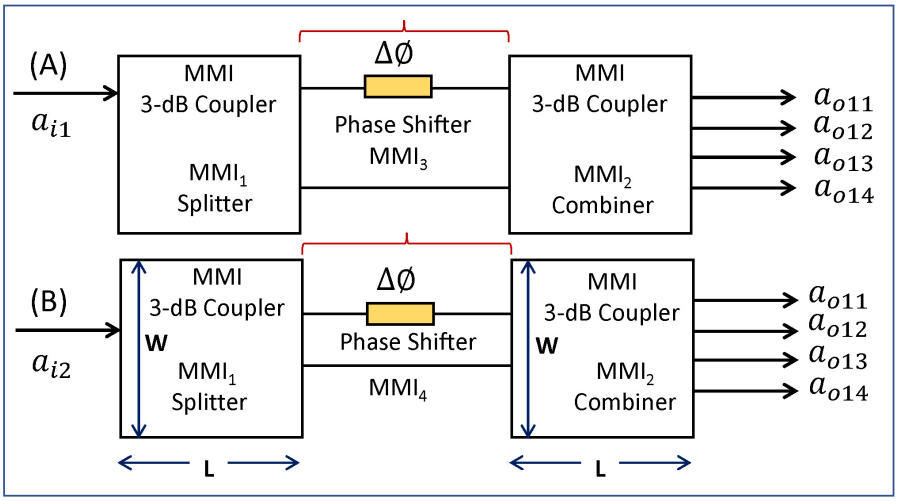

Figure 2. The top view of the MMI_1 and MMI_4, and phase shifters MMI_3 and MMI_4, calculated using MATLAB Mode Solver [18] as well as from FDTD simulation [19], and corresponding waveguide width and access waveguide positions to obtain single self-image at the output port. The device acts as two independent optical switches depending on whether the input is fed through a_{i1} (A) or a_{i2} (B)

For devices with equal length of the phase modulating/shifter and reference arms such as the one considered in this case, a phase shift of π can be introduced with the help of a heater in the modulating arm as the refractive index is temperature dependent as [7]:

$$\Delta\phi = \frac{2\pi}{\lambda} \times \frac{\delta n_{eff}}{\delta T} \times \Delta T \times L_{MMI}(1 + \alpha_L \times \Delta T), \quad (6)$$

where, $\delta n_{eff}/\delta T$ is the thermo-optic coefficient and α_L is the coefficient of thermal expansion and for Si, it is $3.6 \times 10^{-6}/^0$C. At a constant $\delta n_{eff}/\delta T$ and λ, the $\Delta\phi$ is a function of L_{MMI} and ΔT. L_{MMI} is the heating section of the modulating arm. Thermo-optical coefficient of Si is 1.86×10^{-4}K^{-1} at λ = 1550 nm.

A device design based on this mathematical formalism acts as a thermo-optical switch and using this formula, the calculated temperature change, ΔT of 26.77^{o}C is required to achieve a phase shift of π for a 8 μm long modulating MMI.

An electro-thermal joule heating was considered using an Al pad as the electrode. Al was chosen as a heating element because of its large thermal conductivity of 204 W/m^oC at room temperature. The electrode size regarding the heating area was chosen to be 2 μm $\times$ 8 μm to match the size of the modulating/phase shifter arm. The calculated switching voltage of 1.79 V corresponds to the average maximum heating temperature of 50-52^{o}C as a phase shift of π is introduced through the heating pad in the modulating arm with respect to the reference arm. To minimize heat loss and spreading of heat to reference arm and to other parts, a trench is created around the modulating arm as described earlier [7,20,21]. The implementation of this design significantly helps prevent heat spreading and minimize loss by over 90 % as the heat required to drive the switch is directly linked to the device size. The parameters used for the calculation are given in Table 2.

4. Results and Discussions

4.1. Field Distribution in the MMI Couplers /Decouplers

Figure 3 shows the field distribution profile obtained at λ= 1550 nm from FDTD simulation along the length of (a) MMI_1 and (b) MMI_2 (FDTD simulation is a general method to solve Maxwell's partial differential equations in the time domain). In Figure 3(a), the incident power is fed from port 1 (a_{i1}) (see Figs. 1 and 2 for the schematics). As shown in it, for the given configuration, the optical field is tightly confined / concentrated at the center of the waveguide. The field profile suggests that the optical field is not lost through the walls of the waveguide suggesting that some of the light reflected back to the center before reaching the wall. That means, we can reduce the MMI width further (also evident from the field profile). The optical beam emerges from the output ports of the MMI_1 with a power splitting ratio of a_{o1}/ a_{o4} = 0.48/0.47, which closely agrees with our design consideration.

Figure 3(b) shows the field profile of the MMI_2 (Note that MMI_2 = MMI_1) as the incident power is fed from input port 2 (ai_{22}) (again, see Fig 1 for schematics). In this case, the output power is split into 0.46/0.45 ratio. The optimized length of each of the MMI coupler is found to be $L_{MMI1,2}$ = 140 μm. The length of the MMIs are calculated using (2) as: L_{MMI_1} (L_{MMI_2}) = 3 $\times$ L_π/2.

For the device, the insertion loss (IL) is given by:

$$IL = -10 \times log_{10} \times P_{out}/P_{in}, \quad (7)$$

and, the excess loss (EL) is given by:

$$EL = -10 \times log_{10} \times P_{min}/P_{max}. \quad (8)$$

For both the MMIs, the insertion loss and excess losses estimated using FDTD simulation came out to be around 0.65 dB and 0.09 dB, respectively. Note that the L_{MMI} of each MMIs (MMI_1 and MMI_2) was optimized to be 140 μm to achieve this ratio of power splitting, as this ratio and L_{MMI} are directly related to W_{MMI} and n, as shown in (3).

Preprints (www.preprints.org) | NOT PEER-REVIEWED | Posted: 22 April 2019 doi:10.20944/preprints201904.0242.v1

Peer-reviewed version available at Materials 2019, 12, 1555; doi:10.3390/ma12091555

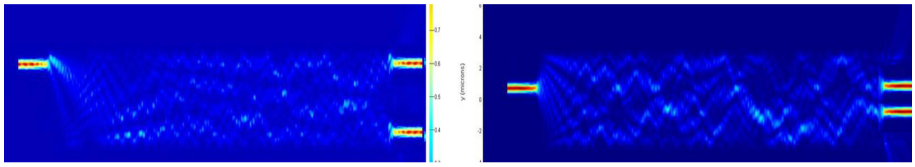

Figure 3. Electric field inside the (a) MMI_1 (input through port a_{i1}) and (b) MMI_2 (input through port a_{i2}). Two-dimensional FDTD numerical method was used to optimize and verify the design [19], as it was shown to produce sufficiently accurate results in simulating devices based on SOI channel waveguides.

By connecting MMI_1 and MMI_2 (each MMI with a length of $L_MMI = 3 \times L_\pi/2$) shown in Fig. 3 together with the MMI phase shifters (MMI_3 and MMI_4) in the linking arms of the MZI configuration as shown in Fig. 1, a two independently operating optical switches, as shown in Fig. 2, can be achieved. Both the phase shifters allow the coupling coefficients of the MMI_2 to vary and tune.

4.2. Field Distribution in the MMI Phase Shifters

The optical field profile of MMI_3 is shown in Fig 4(a). The profile suggests that the optical wave is tightly confined in the center of the waveguide with single-mode propagation and with no noticeable energy loss through side walls. This field profile suggests that the width of this waveguide can be reduced by up to 10 % without sacrificing the operation.

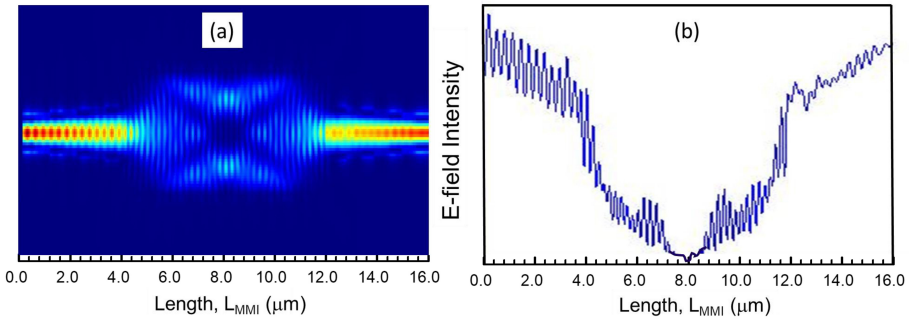

Figure 4. (a) Field profile of a MMI_3 phase shifter without a heater. The 4 μm long tapered access waveguides are connected at both ends of the MMIs to reduce power losses (b) Intensity profile of the 1 $\times$ 1 MMI_3 phase shifter as a function of L_{MMI_3} for a W_{MMI_3} = 2 μm.

The field profile of the light in the linking arm, MMI_4 also showed tightly confined optical filed profile with single-mode propagation and with no seen energy loss through these walls. Note that (MMI_3 = MMI_4). The output to input power ratio is found to be 0.9 to 1.0 (the y-axis label is not shown here), which means, there is a 10 % loss of power. The output power gradually builds up and at the exit, it goes of up to 90 % (Note in Fig. 4(b) the magnitude of the field intensities at L_{MMI} = 8 and 16 μm).

The intensity profile/power profile of the phase-shifter arm as a function of the MMI_3 is shown in Fig 4(b). As shown in it, the power coupling ratio can be tuned/changed by varying the phase shift of the phase modulating arm (i.e., L_{MMI_3}).

4.3. Optical Characteristics of the Switching Device

Figure 5 shows the schematics of the proposed device (cascaded MMI couplers) and the optical switch parameters used for calculation and run FDTD simulations. Each of the optical switches shown in here operate in a binary state (1,0), depending on the output power state either in the bar or in the cross ports of MMI_2.

Preprints (www.preprints.org) | NOT PEER-REVIEWED | Posted: 22 April 2019 doi:10.20944/preprints201904.0242.v1

Peer-reviewed version available at Materials 2019, 12, 1555; doi:10.3390/ma12091555

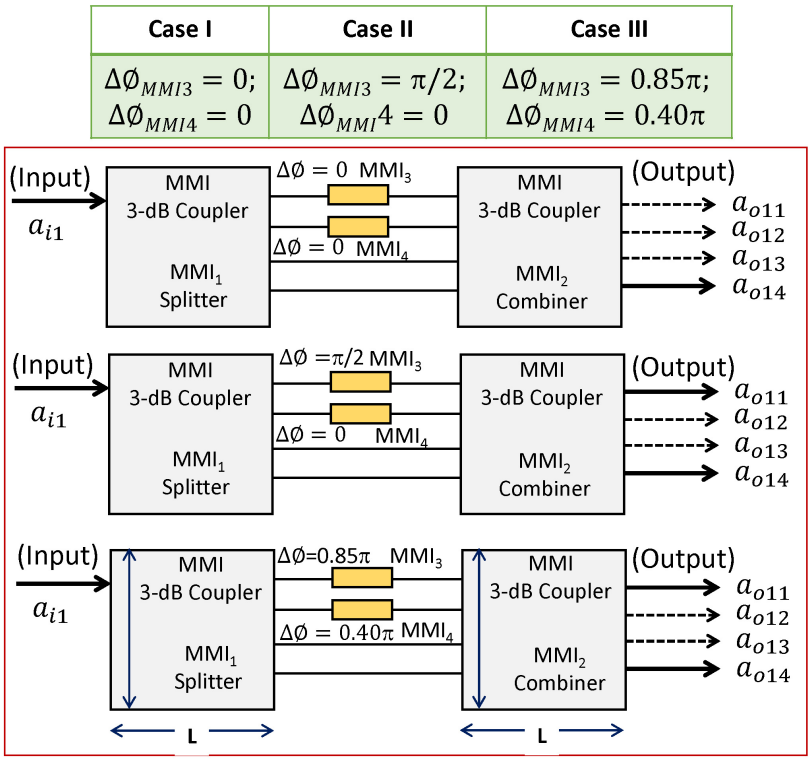

Figure 5. Cascaded MMI device as two independent optical switches: The input is fed through a_{i1} (Case I) $\Delta\phi_{MMI3} = \Delta\phi_{MMI4} = 0$ and (Case II) $\Delta\phi_{MMI3} = \pi/2$ and $\Delta\phi_{MMI4} = 0$ and (Case III) $\Delta\phi_{MMI3} = 0.85\ \pi$ and $\Delta\phi_{MMI4} = 0.4\pi$. The dark bold arrows indicate the light input and output positions.

4.3.1. Case I: $\Delta\phi$= 0, 0 (Heating pads are disabled)

For the light input at port a_{i1}, preliminary simulation results suggested that the normalized output powers from port 1 to 4 are 0, 0, 0, 0.75, respectively when phase shifting is not considered (i.e,$\Delta\phi_{MMI3} = \Delta\phi_{MMI4} = 0$). The excess loss and power imbalance estimated using (7) and (8) are found to be 0.95 dB and 0.1 dB, respectively.

4.3.2. Case II: $\Delta\phi$= $\pi/2$, 0 (Heating pads are enabled)

Upon the introduction of $\pi/2$ phase shift in the first phase shifter, i.e., MMI_3 (i.e, $\Delta\phi_{MMI3} = \pi/2$ and $\Delta\phi_{MMI4} = 0$), the normalized output powers at the output ports are estimated to be 0.48, 0, 0, 0.46, respectively. The excess loss (7) and power imbalances (8) estimated from the FDTD simulation are 0.90 dB and 0.10 dB, respectively.

4.3.3. Case III: $\Delta\phi$= 0.85 π, 0.40 π (Heating pads are enabled)

Upon the introduction of 0.85 π phase shift in the first phase shifter, i.e., MMI_3, and 0.40 π in the second phase shifter (i.e, $\Delta\phi_{MMI3} = 0.85\ \pi$ and $\Delta\phi_{MMI4} = 0.4\pi$), the normalized output powers at the output ports are estimated to be 0.75, 0, 0, 0.10, respectively.

Table 3 lists various switching performance characteristics (output power state for three different phase modulating cases) of the optical switch designed in this work. It shows that the device can be used as multipurpose optical switch. If the phase shifters operate fast enough, then the device may be a very promising building block for use in many types of optical devices.

Preprints (www.preprints.org) | NOT PEER-REVIEWED | Posted: 22 April 2019 doi:10.20944/preprints201904.0242.v1

Peer-reviewed version available at Materials 2019, 12, 1555; doi:10.3390/ma12091555

Table 3. Switching state of the device. The signal is fed at the input port a_{i1}.

Case	$\Delta\Phi$	Output Position	Output State
I	$0, 0$	a_{o11}, a_{o12}, a_{o13}, a_{o14}	0,0,0,0.75
II	$\pi/2, 0$	a_{o11}, a_{o12}, a_{o13}, a_{o14}	0.48,0,0,0.46
III	$0.85\pi, 0.40\pi$	a_{o11}, a_{o12}, a_{o13}, a_{o14}	0.75,0,0,0.10

4.4. Switching Characteristics Tuned by Heater Power Control

The power transmission coefficients of the MMI_1 and MMI_2 couplers obtained from simulation are $\gamma_1^2 = 0.75$ and $\gamma_2^2 = 0.45$, respectively. The transmission coefficient of MMI_2 coupler can be adjusted using the phase shifter arms MMI_3 and MMI_4.

4.5. Output Power State vs Input Driving Power

Switching characteristics of our optimized MMI design are shown in Figure 6, the signal is fed from a_{i1} and then a_{o1} (input of MMI_3). It shows a plot of output power state as a function of heating power, changed in the range of 0 to 2.4 mW. At 1.4 mW and using the resistivity of Si (2.3×10^3 μm), the voltage required to switch the state from 1 to 0 is calculated to be around 1.79 V. The reduction in power loss is almost by a factor of 2 as compared to the conventional phase shifter without the trenches [22,23]. The results suggested that the total device length should be chosen to be 304 μm to achieve the best operation. These results are comparable and consistent with the results estimated using self-imaging theory [6]. The switching performance can be further improved by optimizing the surface area, length/width and thickness of the heating pad, and trench sizes.

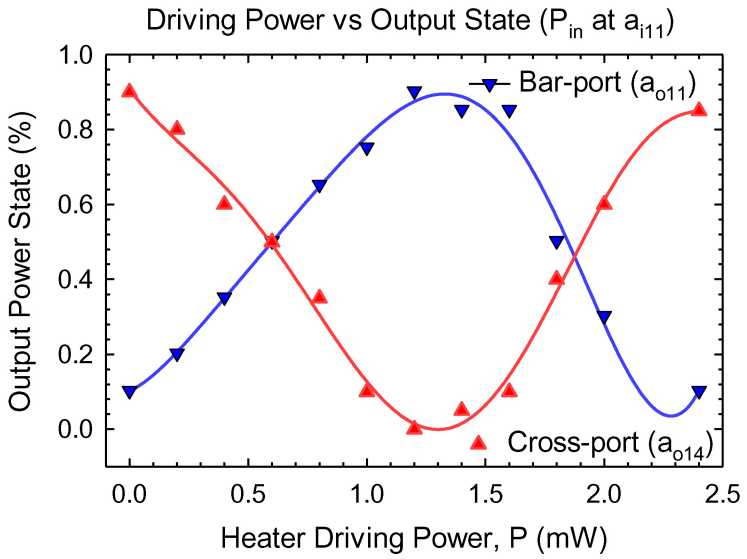

Figure 6. Calculated output power from the output ports of the MMI_2: bar (a_{o11}) and cross (a_{o14}) as a function of the heating power in MMI_3, and input is fed at a_{i1} and a_{o1}. The solid lines are fitted curve using KyPlot [24].

5. Conclusions

In this paper, we theoretically demonstrated the operation of 2×4 multimode interference optical switch with a foot print of 304 μm^2 on SOI technology. The device acts as two independently operating digital switches with improved efficiency and lower footprint, depending on the amount of phase shift introduced by the thermo-optic heaters. As obtained by simulation, the device showed a small insertion loss of around 0.9 dB and excess loss in the range of 0.2 to 0.7 dB. Creating a trench around the Al heating pad and isolating the heater from the surrounding media, the device required a small heating power of 1.4 mW and a switching voltage of around 1.79 V [7] to modulate phase

shift from 0 to π. The new heating method offers the possibility of designing low excess loss and low power consumption optical devices on SOI technology. In addition to using as optical switches, these MMI-based devices have a potential to be used for optical interconnects and micro-ring resonator applications. Moreover, the work can be extended to biosensing that can be used to detect various media such as poisonous gas, environmental changes, as well as diseases caused by harmful bacteria and viruses.

Acknowledgments: Acknowledgments: This work was initially performed by the second author, Conrad Rizal, during his PhD days at the University of British Columbia under the supervision of Dr. Nicolas A. F. Jaeger (PhD Adviser). The work was then extended by the first author, Dr. Boris Niraula who did additional calculation, wrote a draft paper, and revised it. The authors thank Drs. Nicolas A. F. Jaeger and Lukas Chrostowski at the University of British Columbia and Dan Deptuck at CMC Microsystems [25] for providing technical support and access to the FDTD software during design, verification, and simulation process. Authors thank Elizabeth Rizal, a visual-arts student at York University, Canada, for designing/sketching Figure 1 for the paper.

Author Contributions: Author Contributions: C.R. conceived, designed, and carried out theoretical simulation and analyzed the result. B.N. analyzed the result and wrote a paper. C.R. reviewed and approved it.

Conflicts of Interest: Conflicts of Interest: The authors declare no conflict of interest.

1. L.H. Bonani. Modeling an optical network operating with hybrid-switching paradigms. *Journal of Microwaves, Optoelectronics and Electromagnetic Applications*, *15*, 275-292, 2016.
2. For EpiPhotonics. Retrieved from *http://www.epiphotonics.com*, (March 18, 2019).
3. R. Gautam, Silicon microring resonator loaded Mach-Zehnder interferometer for low power optical modulation, switching and bio-sensing, *PhD Dissertation*, Yokohama National University, Japan, 1-153, 2014.
4. L. Lu, L. Zhou, S. Li, Z. Li, X. Li, and J. Chen, "4 $\times$ 4 nonblocking silicon thermo-optic switches based on multimode interferometers, *J. Lightwave Technology*, *33*, 857-864, 2015.
5. R. Boeck, M. Caverley, L. Chrostowski, and N. A. F. Jaeger, Experimental demonstration of a silicon-on-insulator high-performance double microring filter using MZI-based coupling, *Optics Letters*, *40*, 276-279, 2015.
6. O. Bryngdahl, Image formation using self-imaging techniques, *J Optical Society of America*, *63*, 416-419, 1973.
7. C. Rizal and B. Niraula, Compact Si-based asymmetric MZI waveguide on SOI as a thermo-optical switch,*J. Optics Communications*, *410*,947-955, 2018.
8. O. Bryngdahl, Self-imaging with an optical tunnel for image formation, *ed: Google Patents*, 1974.
9. J. M. Heaton and R. M. Jenkins, General matrix theory of self-imaging in multimode interference (MMI) couplers, *IEEE Photonics Technology Letters*, *11*, 212-214, 1999.
10. W. Bogaerts, M. Fiers, and P. Dumon, Design challenges in silicon photonics, *IEEE Journal of Selected Topics in Quantum Electronics*, *20*, 4, 1-8, 2014.
11. H. Hamada, Theoretical time-domain study of self-imaging properties in a multimode interference coupler, *Applied optics*, *46*, 3843-3849, 2007.
12. S. He, X. Ao, and V. Romanov. General properties of N $\times$ M self-images in a strongly confined rectangular waveguide, *Applied optics*, *42*, 4855-4859, 2003.
13. L. B. Soldano and E. C. Pennings, Optical multi-mode interference devices based on self-imaging: principles and applications, *J. Lightwave technology*, *13*, 615-627, 1995.
14. G. Berry and S. Burke, Analysis of optical rib self-imaging multimode interference (MMI) waveguide devices using the discrete spectral index method, *J. Optical and quantum electronics*, *27*, 921-934, 1995.
15. M. Bachmann, P. Besse, and H. Melchior, Overlapping-image multimode interference couplers with a reduced number of self-images for uniform and nonuniform power splitting, *Applied optics*, *34*, 6898-6910, 1995.
16. E. Pennings et al., Ultracompact, low-loss directional couplers on InP based on self-imaging by multimode interference. *Applied physics letters*, *59*, 1926-1928, 1991.
17. R. Ulrich and G. Ankele, Self-imaging in homogeneous planar optical waveguides. *Applied Physics Letters*, *27*, 337-339, 1975.

18. A.B. Fallahkhair., Li S. Kai, and T. E. Murphy. Vector finite difference modesolver for anisotropic dielectric waveguides, *Journal of Lightwave Technology*, *26*, 1423-1431, (2008).
19. D. M. Sullivan, S. Mossman, and M. G. Kuzyk, Time-Domain Simulation of Three Dimensional Quantum Wires, *PloS one*, *11*, e0153802, 2016.
20. R. K. Pokharel and C. S. Rizal, Design and characterization of a compact optical device based on Mach-zehnder interferometer in Silicon-on-insulator technology, *15th Annual Meeting of the Pacific Center for Advanced Materials (PCAMM)*, Vancouver, Canada, 2011.
21. C. Rizal and B. Niraula, Nanoscale silicon waveguide based thermo-optic sensor using a compact Mach-zehnder interferometer. *MDPI Photonics*, August 15 2016. *DOI:10.20944/preprints201608.0151.v1*.
22. A. M. Al-hetar, I. Yulianti, A. S. M. Supaat, and A. Mohammad, Thermo-optic multimode interference switches with air and silicon trenches, *J. Optics Communications*. *281*, 4653-4657, 2008.
23. L. Chrostowski and M. Hochberg. Silicon Photonics Design - From Devices to Systems. *Cambridge University Press*, 2015.
24. Yoshioka, Koichi. KyPlot–a user-oriented tool for statistical data analysis and visualization. *Computational Statistics*. *17*, 425-437, 2002.
25. CMC Microsystem. Nano Silicon-on-Insulator Process Technology. Available online:*http://www.cmc.ca/*, 2019.